Stellar Archeology: Identifying Carbon-Enhanced Metal-Poor Stars from Narrow-Band Photometry

Spencer Clark

Department of Physics, University of Notre Dame

Advisor: Dr. Vinicius Placco

April 3, 2018

Abstract

In the study of the chemical evolution of galaxies, stars of the first generations whose light still exists today can provide a wealth of information regarding the nature of the Universe in the period of several hundred million years after the Big Bang. Stars of this variety often have a low *metallicity*, which is the concentration of iron over hydrogen in the atmosphere of the star, and a large carbon abundance, denoted — similarly to metallicity — by the concentration of carbon over iron in the atmosphere of the star. Jointly, these objects are referred to as CEMP (Carbon-Enhanced Metal-Poor) stars. Historically, astronomers have used spectroscopic means to analyze the light reaching Earth from distant stars; however, in this project, the starlight will be analyzed using photometric methods, with the application of several narrow and broad-band filters from the J-PLUS (Javalambre Photometric Local Universe Survey). The J-PLUS filters are effective at isolating the spectral features of the starlight that serve as proxies for metallicity, carbon abundance, and temperature. To streamline the process of selecting stars of interest, a series of artificial neural networks (ANNs) have been and are being created to estimate stellar parameters. These ANNs use non-linear transformations of the magnitudes of synthetic stellar data analyzed through various arrays of photometric filters. Robust artificial neural networks, focused on different stellar characteristics, can increase the efficiency of CEMP star discovery, expanding the knowledge base of the oldest stars in near-field cosmology.

Acknowledgements

I am humbly grateful for this opportunity to perform research in astronomy at the University of Notre Dame. I would like to thank Vinicius Placco and Timothy Beers for including me in the CEMP S-PLUS proposal back in 2016, and allowing me to contribute to the project. Moving forward, Vini has graciously tolerated my inconsistencies and has always had faith in me, which has pulled me back toward the light of the project. I'd like to thank Devin Witten for his generous help with the supporting computer programming and procedural assistance necessary for my research, as well as for general morale boosts. Thank you to the Glynn Family Honors Program and the College of Science for funding my endeavors, specifically over the summer of 2016. Thank you to Nell Collins, Umesh Garg, and all those involved with the Physics Research Experience for Undergraduates (REU) program who made that summer one to remember. Finally, thank you to my parents, for whom I can attribute many of the fortunes and blessings in my life.

Contents

1 Introduction **1**
1.1 Carbon-Enhanced, Metal-Poor Stars . . . 1
1.2 J-PLUS . . . 3

2 Dataset **3**
2.1 SDSS, S-PLUS Filters . . . 3
2.2 Synthetic Spectra . . . 5
2.3 Dataset and Isochrone Curves . . . 6

3 Analysis **8**
3.1 Filter Difference Patterns . . . 8
3.2 Linear Regression Modeling . . . 9
3.3 Artificial Neural Network Modeling . . . 10

4 Summary and Further Perspective **14**
4.1 Summary . . . 14
4.2 Moving Forward . . . 15

5 References **16**

A Sample Code **17**
A.1 Teff ANN in R . . . 17

1 Introduction

1.1 Carbon-Enhanced, Metal-Poor Stars

After the Big Bang and subsequent cooling of the early universe, the first generation of stars coalesced from the relevant matter present in the interstellar medium. These were particularly pure in composition, consisting primarily of hydrogen and helium. Elements lighter than and including iron are synthesized via the nuclear burning in the center of stars during their evolution. Those heavier than iron are created via the rapid neutron-capture process (r-process) or via the the slow neutron-capturing process (s-process); each process is responsible for approximately half the atomic nuclei heavier than iron. One phenomenon responsible for nucleosynthesis is the explosion of massive stars as supernova, which propels matter throughout its surrounding region. The succeeding generation of stars formed from the debris of these explosions contain these heavier elements formed in the "parental" stars. When searching for information on the early universe, a good place to look is at the oldest low-mass stars in existence today, which are often the generations of stars immediately succeeding the initial, purest generation. To align with this, it is believed that a suggestive sign of this longevity is a scarcity of metal within the star — in this case, iron — and an over-abundance of carbon; the presence of such carbon has been suggested as a cooling agent facilitating the formation of these stars (3). The notation used in stellar astrophysics for the abundance of one element with respect to another is: $[A/B] \equiv log_{10}(N_A/N_B)_* - log_{10}(N_A/N_B)_\odot$ (N_A and N_B refer to the numbers of atoms of elements A and B, and $\odot$ refers to the solar value). Metallicity is typically defined as follows (1):

[Fe/H]	Term	Acronym
>+0.5	Super metal-rich	SMR
0.0	Solar	-
<-1.0	Metal-poor	MP
<-2.0	Very metal-poor	VMP
<-3.0	Extremely metal-poor	EMP
<-4.0	Ultra metal-poor	UMP
<-5.0	Hyper metal-poor	HMP
<-6.0	Mega metal-poor	MMP

Table 1: Definitions of metal-poor stars.

Carbon-Enhanced Metal-Poor (CEMP) Stars	
CEMP	[C/Fe] $> +1.0$
CEMP-r	[C/Fe] $> +1.0$ and [Eu/Fe] $> +1.0$
CEMP-s	[C/Fe] $> +1.0$, [Ba/Fe] $> +1.0$, and [Ba/Eu] $> +0.5$
CEMP-r/s	[C/Fe] $> +1.0$ and $0.0 <$ [Ba/Eu] $< +0.5$
CEMP-no	[C/Fe] $> +1.0$ and [Ba/Fe] < 0

Table 2: Definitions of sub-classes of metal-poor stars.

Additionally, metal-poor stars are considered carbon enhanced when astronomers can identify the abundance or scarcity of carbon by interpreting spectroscopic data from the stellar photons. CEMP stars ([C/Fe] $\geq +0.7$) account for at least 80% of all ultra metal-poor stars observed to date (6). CEMP-no stars (which exhibit sub solar abundances of neutron-capture elements; e.g. [Ba/Fe] < 0.0) are believed to be direct descendents of the first massive stars formed after the Big Bang. Further, the discovery of high-redshift carbon-enhanced damped Lyα systems[1], which present qualitatively similar light-element (from C to Si) abundance patterns to those of CEMP-no stars, provides evidence that carbon is an important contributor to the earliest chemical evolution. An open question in the field is whether the presence of carbon is required for the formation of low-mass second-generation stars the type of star in question in this study. By looking at low-mass, long-lived ultra-metal-poor stars that are thought to have formed from the products of metal-free Population III stars, inferences can be made. A lack of heavy metals in the early universe may have prevented the formation of low-mass stars; as a result, these high-mass "parent" stars enriched the spread of material in space with elements heavier than helium, including carbon.

Stars with these characteristics mentioned are useful to astronomers and astrophysicists for a number of reasons. Distinct among those are: the exposition of the nature of the Big Bang, of the nature of the first stars, and the first universal mass function; predictions of the production of elements by supernovae; among others (1). Finding these stars amidst countless neighbors is no easy task; teams of scientists, mine a prime example, are dedicated to identifying these stars.

[1]Damped Lyα (Lyman-alpha) systems are concentrations of neutral hydrogen gas found in the spectra of quasars. More information about Lyα systems in this context can be found in (2).

1.2 J-PLUS

The major objective of this research is to create analysis methods that will ultimately be applied to real data. One survey of particular interest in this regard is called the Javalambre Photometric Local Universe Survey, or J-PLUS. Conducted in the Spanish *Sierra de Javalambre* mountain range at the *Observatorio Astrofsico de Javalambre* (OAJ), J-PLUS will observe 8500 square degrees of the sky using a set of 12 filters, ranging from broad to narrow band (J-PLUS Website). The photometric capabilities of the panoramic camera associated with J-PLUS allow for the mapping of tens of millions of stars in the Milky Way halo, a region of particular interest within the context of CEMP stars. Similarly to S-PLUS, the data collected through J-PLUS will be made "public as a legacy project for the whole scientific community."

2 Dataset

2.1 SDSS, S-PLUS Filters

Similar to the filters on the outside of a camera, which select for specific wavelength ranges of the electromagnetic spectrum, the narrow-band, S-PLUS filters were designed specifically to isolate stellar features that serve as proxies to metallicity ([Fe/H]), carbonicity ([C/Fe]), and effective temperature (T_{eff}). In addition, the Sloan Digital Sky Survey (SDSS) offers broader filters that include five color bands, covering the entire range from the ultraviolet cutoff at 3000 Å to the sensitivity limit of silicon CCDs (charge-coupled devices) at 11000 Å (see Figure 1): *u'* peaks at 3500 Å with "a full width at half maximum" of 600 Å; *g'*, a blue-green band, is centered at 4800 Å and has a width of 1400 Å; *r'* is the red passband, is centered at 6250 Å with a width of 1400 Å; *i'* is a far red filter centered at 7700 Å with a width of 1500 Å; and *z'* is a near-infrared passband centered at 9100 Å with a width of 1200 Å (see below) (4). The wide bandpasses that are particularly characteristic of the SDSS project ensure a high efficiency for faint object detection, covering essentially all relevant wavelengths of light. The S-PLUS and SDSS filters will be used in various modeling techniques for the extraction of stars of interest from spectral data sets. Since the J-PLUS project uses the same filters as those belonging

to S-PLUS, the filters are attributed to both projects interchangeably throughout this paper.

Figure 1 shows the transmission intensity as a function of wavelength for the five SDSS broadpass filters. The colors chosen (purple for uJAVA, green for gSDSS, and a progressively "darker" gradient of red for rSDSS, iSDSS, and zSDSS as their ranges move closer to infrared wavelengths) are meant to roughly correlate to visible light colors at similar wavelengths.

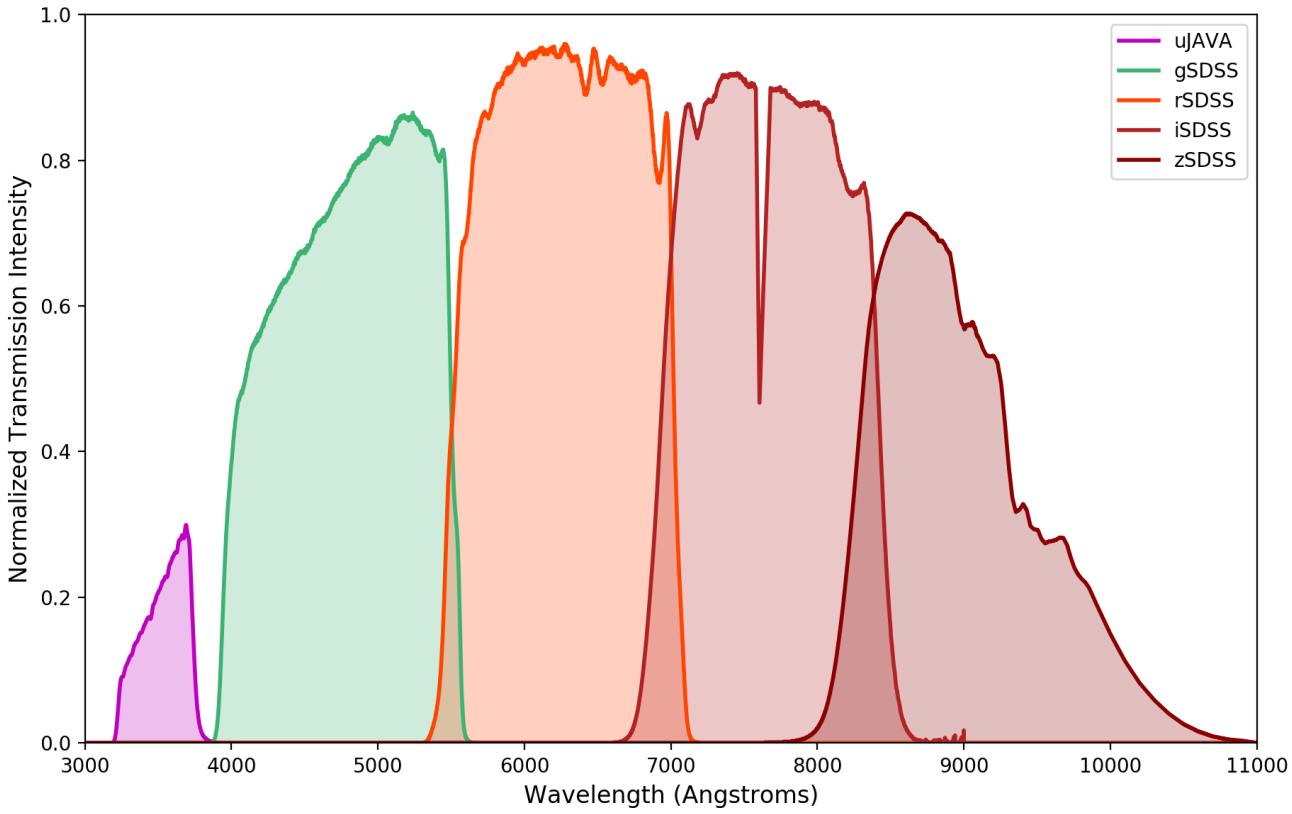

Figure 1: A visual representation of the SDSS broadpass filters.

Figure 2 shows transmission as a function of wavelength for a series of synthetic spectra with three S-PLUS filters (F395, F410, and F430). The filler colors chosen are meant to correlate to visible light colors, similarly to Figure 1. The regions around the intersection of F410 and F430 and immediately succeeding F430 in wavelength are indicators of a CH molecular feature (which provides information for carbon magnitude inferences), while the Ca II K line, which lies within

F395, is sensitive to metallicity. The F410 filter is sensitive to changes in temperature, evidence by changes in the γ absorption feature. Each line at the top of the plot represents a different synthetic stellar spectrum. The red line represents a star with [Fe/H]=-2 and [C/Fe]=0; orange represents [Fe/H]=-3 and [C/Fe]=0; brown represents [Fe/H]=-3 and [C/Fe]=2; and cyan represents [Fe/H]=-4 and [C/Fe]=0. All four have an effective temperature of 5250 K. It is apparent from Figure 2 that the spectrum represented by the brown line, which has a carbon abundance ([C/Fe]) concentration of +2.00, has a more pronounced absorption feature in the area sensitive to carbon abundance. There is a clear gradient in peak magnitude in each filter region of interest. Within the F410 filter, there is very little variation at the most distinct absorption feature; this points to the fact that all four stars have the same effective temperature value, as mentioned above. Compared to the SDSS filters, S-PLUS filters cover a smaller range of optical wavelengths, allowing for the superior isolation of individual spectral features.

2.2 Synthetic Spectra

My responsibility has been to work on ways to streamline the selection process of CEMP stars from photometry using synthetic spectral data sets. To do so, parameter-dependent changes arising from synthetic stellar spectra (see Figure 2) can be isolated and studied to decide how to approach the observational data arising from massive data sets, such as J-PLUS. The synthetic spectra at hand were generated from variations of four key stellar characteristics — effective temperature, logarithmic surface gravity, metallicity, and carbon abundance. From these variations, astronomical magnitudes (e.g. integrated fluxes along a given filter response curve, such as those shown in Figures 1 and 2) are created, which can be used to find trends and make models.

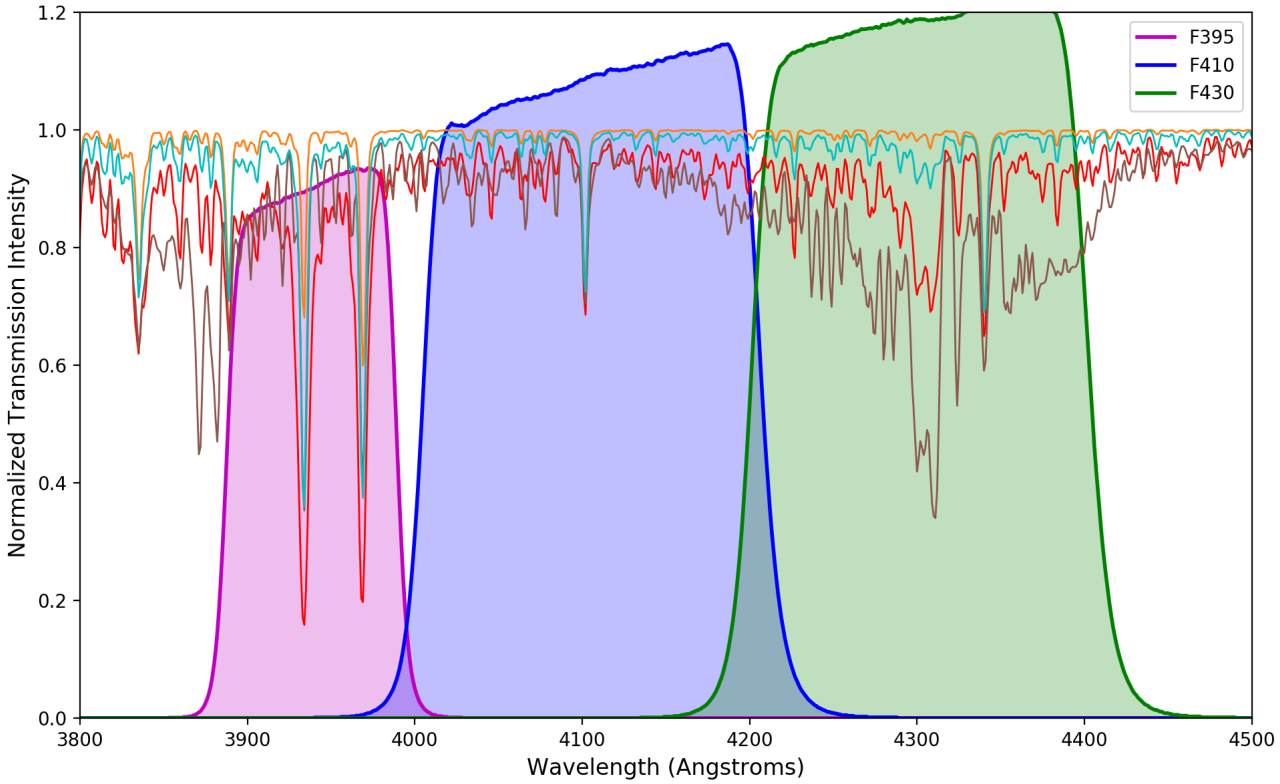

Figure 2: A series of synthetic spectra fitted with S-PLUS filters F395, F410, and F430. Each line at the top of the plot represents a different stellar spectrum. The red line represents a star with [Fe/H]=-2 and [C/Fe]=0; orange represents [Fe/H]=-3 and [C/Fe]=0; brown represents [Fe/H]=-3 and [C/Fe]=2; and cyan represents [Fe/H]=-4 and [C/Fe]=0.

2.3 Dataset and Isochrone Curves

The dataset used in this work was derived from a large set (about 100,000 objects) of synthetic spectra, mentioned above. Restrictions have been made to eliminate unnecessary spectra generated alongside the more replicative, life-like spectra of interest. For instance, spectra with temperatures, carbon abundances, and metallicity ratios that do not align with the typical CEMP portrait are largely trivial in this context and can be dismissed as noise in the generation of the dataset. The desired spectra exist along the isochrone curves shown in Figure 3. The initial cuts made were [Fe/H] < -2.0 and 4000K $\leq T_{eff} \leq$ 7000K. For logarithmic surface gravity, temperature ranges exceeding and preceding the isochrone patterns in Figure 3 were chosen; for example, at Log G = 4,

temperatures 7000K through 5500K were chosen to account for any possible variation. This method was applied at each whole value of Log G, with the intention of capturing any and all viable spectra.

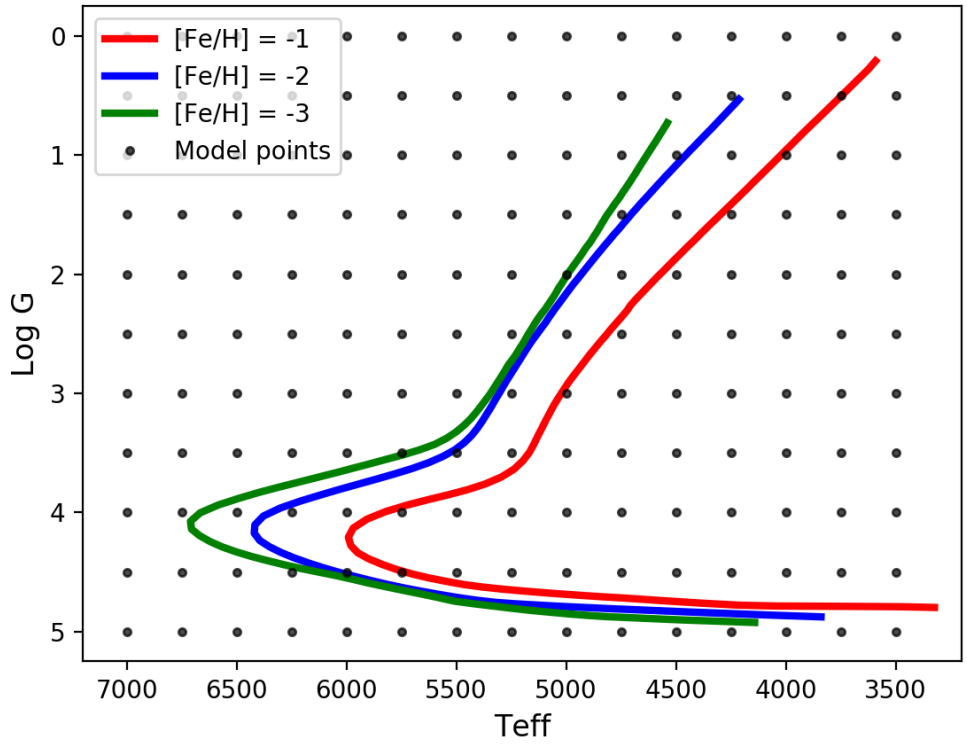

Figure 3: Isochrone curves along which cuts were made. The black dots are artificial stars belonging to the synthetic grid.

Isochrone curves are modifications of stellar representations called Hertzsprung-Russell (HR) diagrams. Typically, HR diagrams plot the relationship between the effective temperatures and luminosities of stars, but here we are interested in the surface gravity factor, Log G, instead of luminosity. As is evident from Figure 3, which depicts three separate stellar evolutionary tracks with common [Fe/H] values (respectively), the metallicity of a star is correlated to its surface gravity and effective temperature, which changes as the star progresses through its evolutionary life stages. These lines in particular represent a star of 0.8 solar masses that evolved for about 12 billion years. Using this connection, we can construct models that effectively target specific stellar parameters of either real and synthetic stars (depending on the application) in order to identify unknown entities

of interest. For example, the cuts listed in the previous paragraph were made to the synthetic spectra because stars with metallicity values of interest fall within those ranges of surface gravity and effective temperature, as evidenced by the isochrone curves. The grid-like points on the plot represent synthetic stars in the dataset; choosing those that fall within the established ranges when building the networks (see below) effectively train the models to sort for the most interesting stars. Their pattern is regular due to their artificial origin. These "stars" are meant to serve as tools of research; having predictable, easily delineated and evenly spaced parameter values may detract from the element of natural authenticity, but the salience and ease of operation from a computational standpoint in certainly increased.

There were issues with the synthetic grid that were not discovered until after much of the initial network progress had been made in the summer of 2016 (see section 3.3). Many of the spectra were unrealistic or fundamentally broken — a result likely stemming from some error in their formulation. We were able to test the nets with the new, "clean" synthetic grid, the results of which were used to draw conclusions about the varying levels of promise of the modeling methods.

3 Analysis

3.1 Filter Difference Patterns

Initial analysis of the cut data set began with an exercise looking into the relationship between filter magnitude differences, additionally separating the stars by key characteristics like gravity and carbon abundance. From these distinctions, significant trends can be seen along carbon abundance lines (see Figure 4). The colors represent: $[C/Fe] \leq 0$ (Yellow), $0 < [C/Fe] \leq 0.4$ (Green), $0.4 < [C/Fe] \leq 0.7$ (Black), $0.7 < [C/Fe] \leq 1.5$ (Blue), and $[C/Fe] > 1.5$ (Red). The subplots of Figure 4 split the spectra into two categories: those with a Log G value less than or equal to 2 on top and those with a Log G value greater than two on the bottom. While the filter combinations alone were not able to capture the behavior of interest, this exercise pointed us towards the possibility of success within linear regression. This possibility stems from the fact that there seems to be a relationship

between the scalar dependent variable ([C/Fe]) and the explanatory, independent variable (filter combinations).

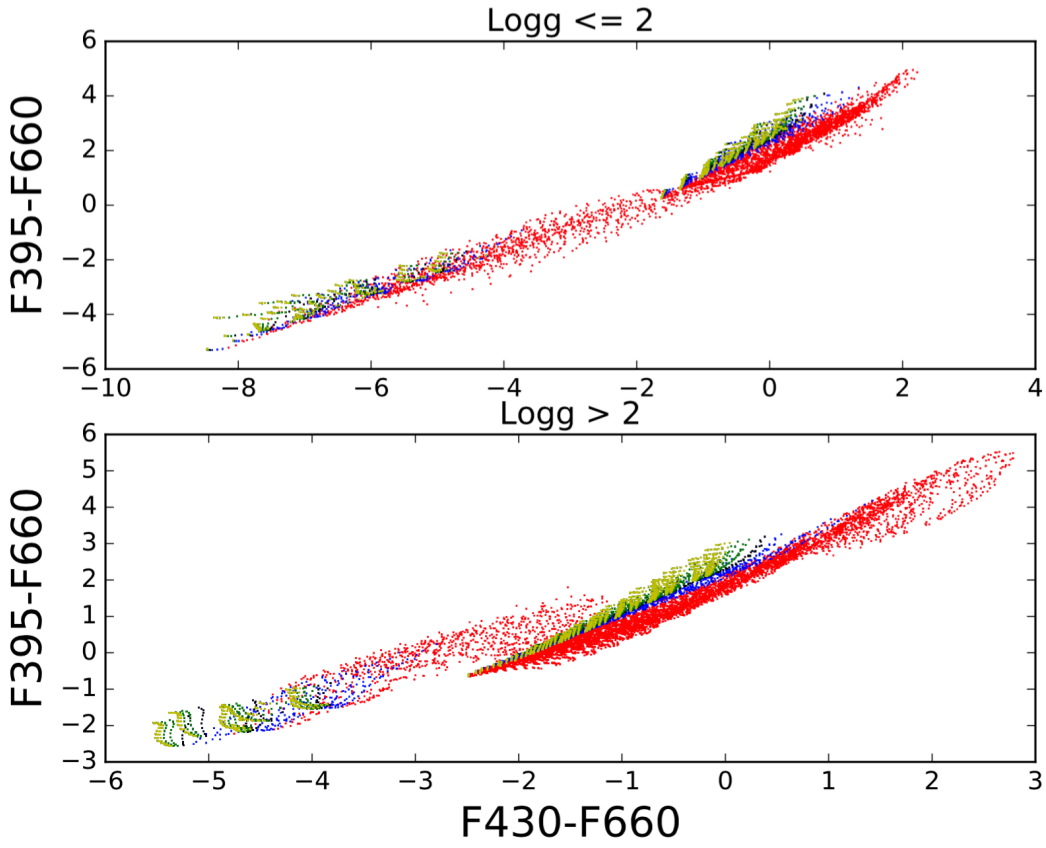

.

Figure 4: Synthetic spectra sorted by graph based on Log G value and by color based on carbon abundance

3.2 Linear Regression Modeling

If a model can be found that effectively predicts the stellar parameters and carbon abundances from the J-PLUS magnitudes, sets of observational data can be efficiently sorted, eliminating noise from consideration and expediting the process, which can allow for a wider breadth of stars to be analyzed with the conservation of time and resources. It is important for the model to show correlation with the original spectra, as it is important for the artificial neural network results to show correlation with the test and training sets (next section). Using various combinations of filter magnitudes as parameters,

linear regression models were computed using the *ols* module within the larger python-oriented *statsmodels* module, where coefficients paired with the input parameters are linearly generated to create a model. We were successful in creating linear models for temperature, metallicity, and carbon, with the most success in temperature (success determined by residual statistics and r-squared value of correlation between synthetic and predicted sets). It was decided that a linear regression model could be useful, but likely would not be robust enough for our project. In Figure 5, the residual statistics are: mean = 0.00, variance = 0.78, and sigma (standard deviation) = 0.88.

Looking at Figure 5, the top-most subplot shows the predicted [C/Fe] values (using the filter combinations listed in the title of the figure) as a function of the actual synthetic spectral [C/Fe] values. The middle subplot is a modified visualization of the information in the top-most subplot, here instead depicting the difference in predicted and actual values as a function of the actual values. Finally, the bottom-most subplot depicts a histogram of the frequency of points in the second subplot. It appears that the actual and predicted values are roughly correlated (see residual statistics), as evidenced by the linearity in the top-most subplot and the uniform Gaussian curve in the bottom-most subplot.

3.3 Artificial Neural Network Modeling

In addition to a linear regression route, the employment of the artificial neural net (ANN) was considered to be a more robust approach, able to interpret the variability of observational data in a more effective manner than the linear counterpart. As defined by Dr. Robert Hecht-Nielsen, a neural network is (UW Networks):

> "...a computing system made up of a number of simple, highly interconnected processing elements, which process information by their dynamic state response to external inputs."
> In "Neural Network Primer: Part I" by Maureen Caudill, AI Expert, Feb. 1989

ANNs are processing tools that resemble the neuronal structure of the mammalian cerebral cortex on a small scale. Typically organized in layers, which are made up of a number of interconnected nodes containing respective activation functions, neural networks consist of an array of interconnects

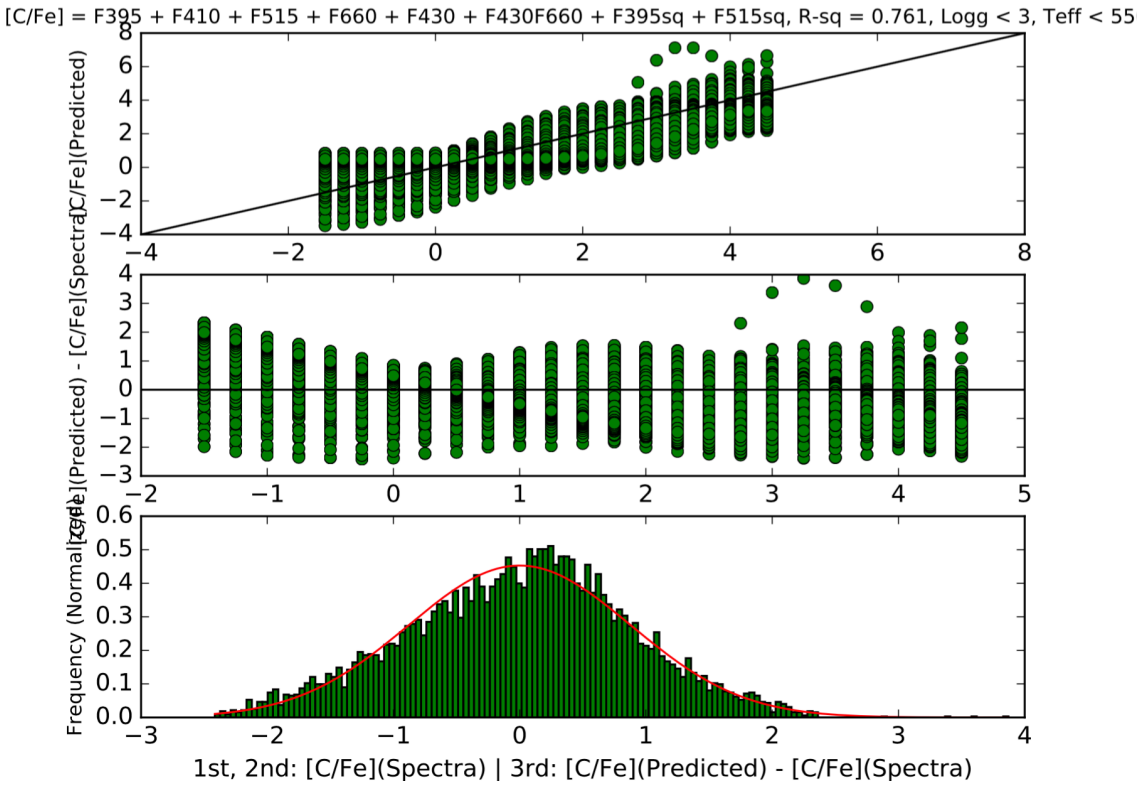

Figure 5: A Linear Regression Model [C/Fe].

that accept pattern information at the initial ("input") layer, processes the information via the inner "hidden" layer, which communicates under weighted conditions, and finally present the result via the "output" layer. This architecture is visible in Figure 6. The weights of the inner layers are modified according to input patterns presented to the network. As a result, the network is able to "learn" from repetitious pattern exposure. A modified version of backpropagation with a sum of squares error function was used as a learning tool. Backpropagation creates a downward gradient within the solution's vector space toward a global minimum, driving the network toward the most efficient and accurate solution.

An ANN package belonging to the statistical language R was implemented using a randomized half of the pre-cut synthetic spectra set as the training set for the ANNs, and its complementary half as the testing set. With the filters and colors chosen, as done before in the case of linear regression,

the nets were created. Figure 6 displays a visualization of an ANN designed for temperature forming from a training set. From here, the resulting predicted values (in Figure 7, T_{eff}) gleaned from the filters were statistically compared to the synthetic training set. Similarly, the test set was run through the ANN to test its resiliency with a new set of data; statistical comparisons between the test set and the calculated values can also be found in Figure 7. Other combinations of filters have been used in ANNs not shown for the sake of brevity, but this method appears successful for modeling temperature.

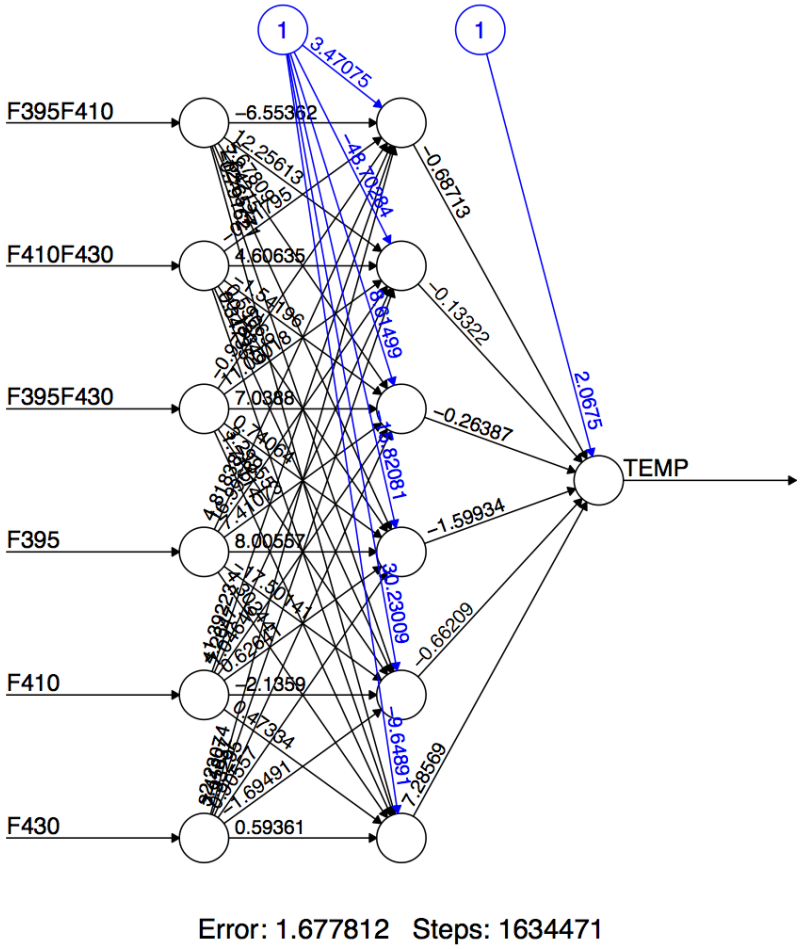

Figure 6: A visualization of a training ANN for T_{eff} in R.

Figure 6 is a visualization of a training ANN for effective temperature in R. The code in Appendix A is an example of the script used to generate such an ANN. Six filters, some of which are combinations, are used as an input layer. The information from the data set in question is processed

in the hidden layer, communicating under weighted conditions as shown by the magnitude-assigned arrows in black and blue. Finally, the resultant set of values is produced via the output layer.

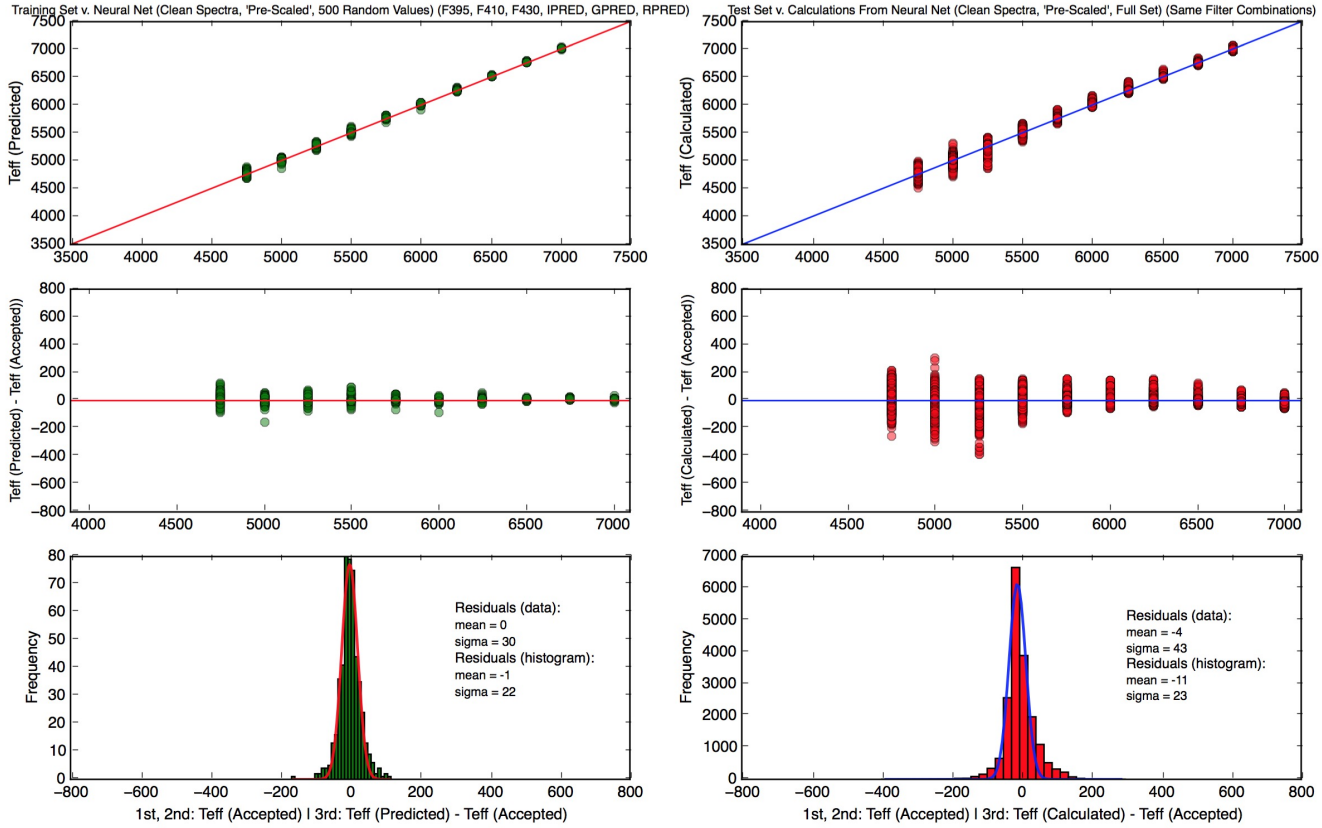

Figure 7: Training and test spectral sets corresponding to an R-coded ANN based on the effective temperature parameter. The script included pre-scaling measures and the data set was cleaned of corrupt spectra.

Figure 7, analyzed with greater scrutiny, depicts the results of an effective temperature ANN. On the left, the three subplots show the relationships between a training set of 500 random values from the synthetic spectra (corrupt spectra removed and all spectra pre-scaled[2]) and the neural net outputs using F395, F410, F430, IPRED, GPRED, and RPRED filters (the latter-most three are SDSS filters renamed). The upper-most subplot shows the predicted effective temperature values

[2]The inputs of the ANN have magnitudes ranging from 10-20, while the outputs (effective temperatures) range from 4000 to 7000. The input values must be scaled for the coherent proceeding of the network. This is done by subtracting the mean and dividing by the standard deviation of the set of all input effective temperatures, in the case presented here.

from the ANN as a function of values ("accepted") from the random training set. The middle subplot shows the difference between the predicted and accepted values as a function of the accepted values. The bottom-most subplot shows the frequency of the differences in the middle subplot in the form of a histogram, fitted to a normal distribution and evaluated for residual statistics values. On the right, the three subplots depict similar information as those on the left, but with a test set consisting of all synthetic spectra of interest (i.e. subject to isochrone curve cuts). Despite an increased variability between the test set and the accepted effective temperature values, the sigma values were low enough (σ=30K, 43K respectively) to affirm the success of this combination of filters.

Attempts to use an R-coded ANN to select for the other parameters in question — namely metallicity, carbon abundance, and surface gravity — were unsuccessful. The computation, even when allowed to run indefinitely on remote processor clusters, consistently failed to converge. Because of this, we have been considering the employment of different ANN packages outside of the R language. One of particular interest is a Python-based package.

4 Summary and Further Perspective

4.1 Summary

From the results of our modeling, the ANN approach shows the most promise regarding its ability to increase efficiency in the search for CEMP stars — here, with the J-PLUS survey. Looking at residual values, the sigma values of the ANN method applied to effective temperature (σ=30K, 43K) were lower than the value for the linear regression model (σ = 0.88); 40K in a conversation dealing with temperatures in the thousands of Kelvin is quite small compared to 0.88 in a conversation of single digit carbon abundance values. On a personal level, I have gained experience problem solving in a computer science context; working with graduate students and with peers in a team setting; coding in Python, R, and Unix; and learning about general themes in near-field astronomy, as well as in the smaller niche of stellar archaeology, as it has been called. The initial success of ANNs has been used to further the research of my colleagues as the probe into the nature of CEMP stars.

4.2 Moving Forward

Further work to be done in this vein of near-field CEMP astronomy is largely centered on the development of robust artificial neural networks for the other stellar characteristics. As mentioned above, we believe that a Python network module may prove to be more robust and could provide results when sorting for the other stellar parameters, namely surface gravity, carbon abundance, and metallicity. Additionally, new filter combinations may be implemented as modified ANNs are formulated; there has been an interest in whether previously used combinations, like those used in the *Skymapper* survey, prove effective under this method (5). The ultimate goal, as stated in the introduction, is to apply these methods to the J-PLUS survey of stars in order to identify those that express CEMP characteristics. Once identified, these CEMP candidates will be analyzed again with high-resolution spectroscopy in order to determine their full chemical abundance patterns. These can be compared with theoretical predictions for chemical evolution after the Big Bang, which will help increase the clarity of our resolution of the early Universe.

5 References

References

[1] Beers, T. C., & Christlieb, N. 2005, ARA&A, 531-535

[2] Ryan Cooke, Max Pettini, Michael T. Murphy; A new candidate for probing Population III nucleosynthesis with carbon-enhanced damped Ly systems, Monthly Notices of the Royal Astronomical Society, Volume 425, Issue 1, 1 September 2012, Pages 347354, https://doi.org/10.1111/j.1365-2966.2012.21470.x

[3] Frebel, A. 2010, arXiv:1006.2419v1

[4] Fukugita, M., Ichikawa, T., Gunn, J. E., et al. 1996AJ, 111.

[5] Keller, S. C., Schmidt, B. P., Bessell, M. S., et al. arXiv:astro-ph/0702511v1 20 Feb 2007 p.9

[6] Placco, V. M., Frebel, A., Beers, T.C., et al. 10 December 2016, doi:10.3847/0004-637X/833/1/21, p.1-2

[J-PLUS Website] Javalambre Photometric Local Universe Survey. J-PLUS, Javalambre Photometric Local Universe Survey, www.j-plus.es/survey.

[UW Networks] A Basic Introduction To Neural Networks. Department of Computer Sciences University of Wisconsin-Madison, pages.cs.wisc.edu/ bolo/shipyard/neural/local.html.

A Sample Code

A.1 Teff ANN in R

```
require(neuralnet)

require(nnet)

set.seed(250)

load(".RData")


TRAIN<-read.table(file="TRAIN_safe_abr.csv", header=TRUE, sep=",")


#Scaling code

MEAN <- mean(TRAIN$Teff)

SCALE <- sd(TRAIN$Teff)


TEMP <- (TRAIN$Teff - MEAN)/SCALE


F395 <- scale(TRAIN$F395)

F410 <- scale(TRAIN$F410)

F430 <- scale(TRAIN$F430)

GPRED <- scale(TRAIN$GPRED)

RPRED <- scale(TRAIN$RPRED)

IPRED <- scale(TRAIN$IPRED)


# The newly created vectors need to be stuffed into a table before

# They can be used with neuralnet

TRAIN_SET <- data.frame(TEMP,F395,F410,F430,GPRED,RPRED,IPRED)
```

```
#Hidden is the number of nodes in the hidden layer. One or two hidden layers
# should suffice
n4_t_2 <- neuralnet(TEMP~F395+F410+F430+GPRED+RPRED+IPRED, data=TRAIN_SET, hidden=6,
algorithm="rprop+",act.fct="tanh", stepmax=1e8)



# When it's complete, the results can be written to a file
# These are the predictions it made for TEMP using the TRAINING set
write((unlist(n4_t_2$net.result)*SCALE+MEAN), file="n4_t_2_2.dat", sep="\n")

save.image(RDATA)

#~~~~  TEST  ~~~~
TEST<-read.table(file="safe.csv", header=TRUE, sep=",")

#Scaling code
MEAN <- mean(TEST$Teff)
SCALE <- sd(TEST$Teff)

TEMP <- (TEST$Teff - MEAN)/SCALE

F395 <- scale(TEST$F395)
F410 <- scale(TEST$F410)
F430 <- scale(TEST$F430)
GPRED <- scale(TEST$GPRED)
RPRED <- scale(TEST$RPRED)
```

```
IPRED <- scale(TEST$IPRED)

# The newly created vectors need to be stuffed into a table before they can
# be used with neuralnet
TEST_SET <- data.frame(TEMP,F395,F410,F430,GPRED,RPRED,IPRED)



# Hidden is the number of nodes in the hidden layer. One or two hidden layers
# should suffice

PREDICTION <- compute(n4_t_2, TEST_SET[,2:7])



# When it's complete the results can be written to a file
# These are the predictions it made for TEMP using the TRAINING set
write(unlist(PREDICTION$net.result)*SCALE+MEAN, file="test_compute4_t_2_2.dat", sep="\n")

save.image("RData")
```